Chemical Science

ROYAL SOCIETY OF CHEMISTRY

EDGE ARTICLE

View Article Online
View Journal | View Issue

Cite this: *Chem. Sci.*, 2024, **15**, 2211

All publication charges for this article have been paid for by the Royal Society of Chemistry

Received 12th October 2023
Accepted 1st January 2024

DOI: 10.1039/d3sc05403a

rsc.li/chemical-science

Untangling ancillary ligand donation *versus* locus of oxidation effects on metal nitride reactivity†

Samyadeb Mahato, Warren VandeVen, Gregory A. MacNeil, Jason M. Pulfer and Tim Storr *

We detail the relative role of ancillary ligand electron-donating ability in comparison to the locus of oxidation (either metal or ligand) on the electrophilic reactivity of a series of oxidized Mn salen nitride complexes. The electron-donating ability of the ancillary salen ligand was tuned *via* the *para*-phenolate substituent (R = CF_3, H, *t*Bu, O^{i}Pr, NMe_2, NEt_2) in order to have minimal effect on the geometry at the metal center. Through a suite of experimental (electrochemistry, electron paramagnetic resonance spectroscopy, UV-vis-NIR spectroscopy) and theoretical (density functional theory) techniques, we have demonstrated that metal-based oxidation to $[Mn^{VI}(Sal^R)N]^+$ occurs for R = CF_3, H, *t*Bu, O^{i}Pr, while ligand radical formation to $[Mn^{V}(Sal^R)N]^{+\bullet}$ occurs with the more electron-donating substituents R = NMe_2, NEt_2. We next investigated the reactivity of the electrophilic nitride with triarylphosphines to form a Mn^{IV} phosphoraneiminato adduct and determined that the rate of reaction decreases as the electron-donating ability of the salen *para*-phenolate substituent is increased. Using a Hammett plot, we find a break in the Hammett relation between R = O^{i}Pr and R = NMe_2, without a change in mechanism, consistent with the locus of oxidation exhibiting a dominant effect on nitride reactivity, and not the overall donating ability of the ancillary salen ligand. This work differentiates between the subtle and interconnected effects of ancillary ligand electron-donating ability, and locus of oxidation, on electrophilic nitride reactivity.

Introduction

Transition metal complexes featuring terminal nitride (N^{3-}) ligands have attracted significant interest due to their potential role in nitrogen fixation,[1–4] stoichiometric nitrene transfer reactions,[5–7] catalytic applications,[8,9] and their utility in materials chemistry.[10–12] In the context of nitrogen fixation, the electronic structure and reactivity of bioinspired Fe nitride complexes have been extensively studied,[13–27] along with recent investigations of synthetic FeMo cofactors that have provided insight on the stability and reactivity of activated Fe–N species.[28,29] The reactivity of terminal nitride complexes is often rationalized based on the nucleophilic or electrophilic nature of the nitride ligand, which is influenced by the specific metal, oxidation state, and the nature of the ancillary ligands.[30–32] Notably, late transition-metal nitrides can exist as isolated or transient intermediates, exhibiting electrophilic reactivity through low energy M≡N π* antibonding orbitals.[33–45] Conversely, early transition-metal nitrides are generally more stable[46–48] and in some cases demonstrate nucleophilic reactivity *via* filled M≡N π orbitals or the nitride lone pair.[49–53] Certain metal nitride complexes have been reported to exhibit ambiphilic reactivity, highlighting that subtle modifications to the coordination environment and/or redox changes can enable diverse reactivity.[35,54–56] Previous studies by Mayer *et al.*[57,58] and Lau *et al.*[59] have elucidated how changes in ancillary ligands can impact nitride reactivity, work by Holland *et al.* demonstrated that oxidation of both the metal and ancillary ligand (from amide to nitroxide) led to a change from nucleophilic to electrophilic nitride reactivity,[60] and a recent study by Burger and co-workers showed that oxidation of an Ir nitride complex resulted in insertion of the nitride into an aromatic C–C bond of ferrocene.[61] Further investigation into the effects of subtle changes in electronic structure on nitride reactivity will yield valuable insight for new reactivity applications.

We have shown that the electronic structure of oxidized nitridomanganese(v) salen complexes (where "salen" represents N_2O_2 bis-phenolate bis-Schiff-base ligands) can be tuned through the adjustment of the electron-donating ability of the *para*-R phenolate substituents, while preserving the geometry at

Department of Chemistry, Simon Fraser University, Burnaby, British Columbia, V5A 1S6, Canada. E-mail: tim_storr@sfu.ca

† Electronic supplementary information (ESI) available: Full experimental details, X-ray structures, CV data, UV-vis-NIR data, kinetics, EPR analysis, ^{1}H NMR, ^{31}P NMR and ESI-MS, reactivity profiles, and DFT calculation data including molecular orbitals, spin densities, NBO analysis, NPA analysis, transition state geometries, calculations and free energy profiles; theoretical eyring plot, crystallographic data for **Mn(Sal^H)N**, DFT metrical parameters. CCDC 2298460. For ESI and crystallographic data in CIF or other electronic format see DOI: https://doi.org/10.1039/d3sc05403a

the metal center.[62,63] Salen ligands exhibit redox-active behavior, enabling oxidation or reduction at the ligand in competition with the metal.[64–70] Upon oxidation, we and others observed the formation of a Mn^{VI} salen nitride, leading to the activation of the Mn≡N bond, and rapid nitride homocoupling to generate N_2, even at low temperatures.[62,71,72] Intriguingly, the introduction of electron-donating substituents (R = NMe_2) at the *para* position of the salen ligand leads to the formation of a ligand radical, which is stable in solution at 298 K.[62] Additionally, a separate study has reported an isolable Mn^{VI} nitride complex with a tetraamido macrocyclic ligand (TAML), which exhibits relatively slow nitride homocoupling at 298 K.[54] Recent reports have utilized Mn salen nitrides to explore the hydrogen atom bond dissociation free energy of associated imido complexes,[73] the generation of ammonia through proton-coupled electron transfer[10,74,75] and their application as catalysts for ammonia oxidation.[76] Intrigued by the difference in behaviour of the Mn salen nitride complexes upon oxidation, we endeavoured to probe the reactivity difference for an expanded series of oxidized nitridomanganese(v)salen complexes with phosphines and to characterize the resulting phosphoraneiminato adduct. In our previous work with a smaller series of oxidized Cr analogues, we found that while the Cr(vi) nitride complexes reacted with phosphine, a ligand radical derivative did not, and it was unclear whether the locus of oxidation or the electron-donating ability of the salen ligand was primarily responsible for this abrupt reactivity change.[77] Factors such as the nature of the ancillary ligands, steric effects, metal oxidation state and overall charge of the complex can influence the analogous oxygen atom transfer reaction efficiency of oxo ligands with triaryl phosphines.[78–83] Two-electron nitrogen transfer reactions of metal nitride complexes with phosphines to form the phosphoraneiminato moiety (–N=PR_3) are well known,[30] and in the majority of cases the phosphine acts as a nucleophile;[25,55,84–86] in some exceptional instances nitride lone pair donation into the phosphine LUMO (generally, a P–C σ*) gives rise to a dual nature transition state.[87] Herein, we questioned whether the locus of oxidation, or alternatively the electron-donating ability of the salen ligand, is the major driving factor in the reactivity differences for a series of $[Mn(Sal^{R})N]^{+}$ complexes with triarylphosphines (Scheme 1), and how the change in locus of oxidation, from metal to ligand, would map against the ligand Hammett parameter, and thus donating ability, of the salen ligand.

Results and discussion

Synthesis and characterization

To investigate the role of the ligand electronics and locus of oxidation on nitride reactivity, six nitridomagnanese(v) salen complexes were prepared with a range of ancillary ligand electron-donating ability. **Mn(Sal^{CF3})N**, **Mn(Sal^{tBu})N**, **Mn(Sal^{OiPr})N** and **Mn(Sal^{NMe2})N** have been previously synthesized.[62,63] For the two new complexes, unsubstituted **Mn(Sal^{H})N** was prepared by the reaction of corresponding manganese chloride salt with NH_4OH as reported by Carreira and coworkers (Scheme S1 and Fig. S1†).[7] On the other hand, **Mn(Sal^{NEt2})N** was prepared by the photolysis of the precursor manganese–azido complex to avoid a difficult purification procedure (Schemes S2, S3 and Fig. S2†). X-ray quality crystals of **Mn(Sal^{H})N** were obtained by layering hexanes over a concentrated dichloromethane (CH_2Cl_2) solution (Fig. S3 and Table S1†). The expected pseudo square pyramidal geometry with a nitride Mn–N bond distance of 1.517 Å was observed, analogous to other reported Mn salen nitrides.[62,63]

Electrochemistry

The redox properties of the two new complexes were analyzed by cyclic voltammetry (CV) experiments at 298 K under a N_2 atmosphere. The voltammogram of **Mn(Sal^{H})N** displayed a partially reversible redox process with an $E_{1/2}$ = 0.28 V (*vs.* Fc^{+}/Fc), attributed to metal-based oxidation (*vide infra*) (Fig. 1A and S4A†). The partial reversibility at 298 K is indicative of nitride homocoupling observed in analogous Mn(vi) complexes.[62,71] In contrast, **Mn(Sal^{NEt2})N** showed two overlapping quasi-reversible redox processes which were resolved by differential pulse voltammetry (DPV) to afford redox potentials at $E_{1/2}{}^{1} = -0.15$ V and

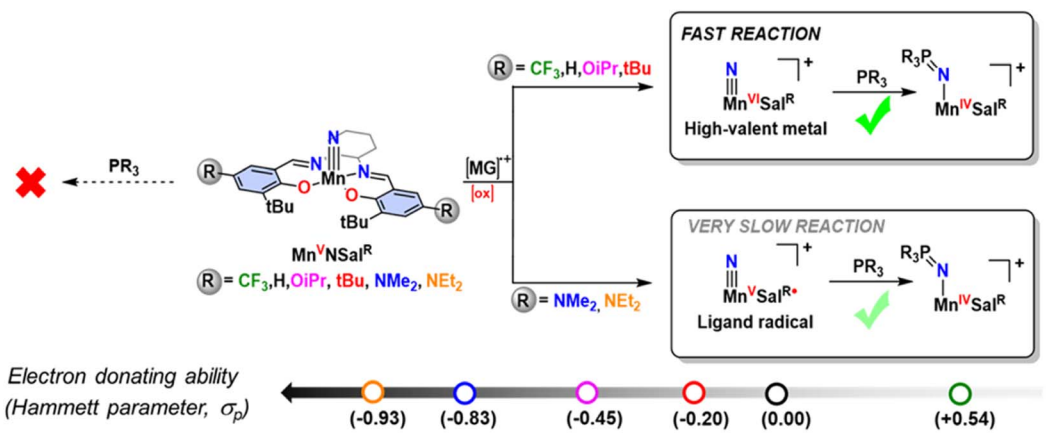

Scheme 1 Locus of oxidation dependent electrophilic reactivity of a series of oxidized Mn-Salen-Nitrides incorporating different salen ligand *para*-ring substituents. $[MG]^{+\bullet}$ = magic green chemical oxidant.

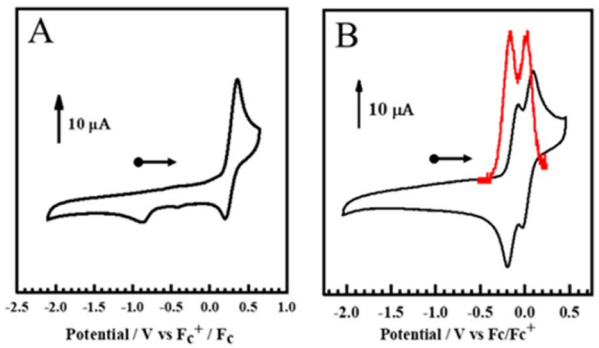

Fig. 1 (A) Cyclic Voltammogram of **Mn(Sal^{H})N** and (B) **Mn(Sal^{NEt2})N**. Conditions: 1.0 mM complex; 0.1 M $^{n}Bu_4NClO_4$; scan rate: 100 mV s^{-1}; T = 298 K; CH_2Cl_2. DPV curve in red.

$E_{1/2}{}^2 = -0.01$ V respectively (Fig. 2B and S4B†). The electrochemistry data is consistent with two successive oxidations of the phenolate moieties at low potentials for the most electron-donating substituents, as observed for both **Mn(Sal^{NMe2})N** and **Cr(Sal^{NMe2})N**.[62,77] A small ΔE_{ox} ($E_{1/2}{}^2 - E_{1/2}{}^1$) value of 140 mV indicates minimal electronic coupling between the redox-active phenolates, supporting a localized ligand radical for **[Mn^{V}(Sal^{NEt2})N]$^{\bullet+}$** upon one-electron oxidation (Table 1).[62] We investigated the degree of disproportionation of the mono-oxidized form at 193 K (conditions relevant to the reactivity studies, see

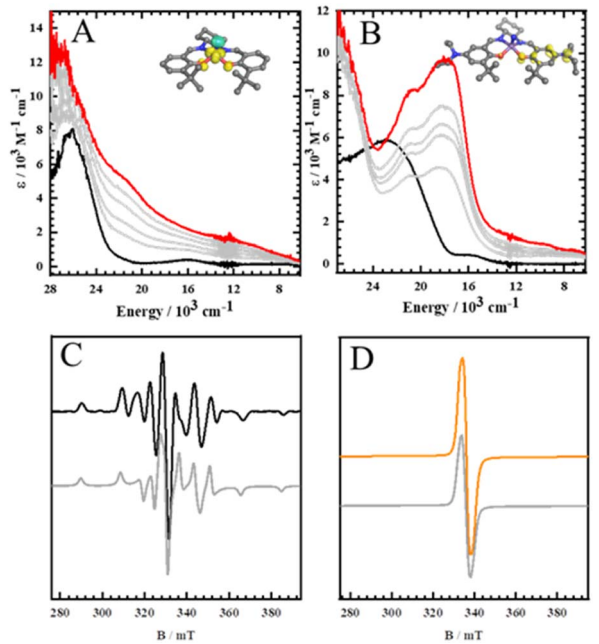

Fig. 2 Oxidation titration data for (A) **Mn(Sal^{H})N** and (B) **Mn(Sal^{NEt2})N** monitored by UV-vis-NIR spectroscopy. Black: neutral; red: oxidized; intermediate grey lines were measured during the oxidation titrations with $[N(C_6H_3Br_2)_3]^{+\bullet}[SbF6]^-$, insets: spin density plot of the oxidized complexes. Conditions: CH_2Cl_2, 0.1 mM, 193 K (see Experimental section for calculation details) X-band EPR spectra of frozen (C) [Mn(SalH)N]+ and (D) **[Mn(Sal^{NEt2})N]$^+$** samples respectively. Simulated spectra are represented by grey lines. Conditions: frequency = 9.38 GHz; power = 2.0 mW; modulation frequency = 100 kHz; modulation amplitude = 0.6 mT; CH_2Cl_2, T = 20 K.

Table 1 $E_{1/2}$ of the Mn(Sal^{R})N complexes (*vs.* Fc^+/Fc) and correlation with Hammett parameter (σ_p). Peak-to-peak separation given in parenthesis [[a] = ref. 62. [b] = ref. 63. [c] = ref. 90]

Compound	$E_{1/2}{}^1$ (V)	$E_{1/2}{}^2$ (V)	σ_p^c
Mn(Sal^{CF3})N	0.42		0.54
Mn(Sal^{H})N	**0.28 (0.16)**		**0.00**
Mn(Sal^{tBu})N	0.23[a]		−0.20
Mn(Sal^{OiPr})N	0.21[b]		−0.45
Mn(Sal^{NMe2})N	−0.10[a]	0.05	−0.83
Mn(Sal^{NEt2})N	**−0.15 (0.14)**	**−0.01 (0.14)**	**−0.93**

ESI† for details), calculating that only *ca.* 1.5% **[Mn^{V}(Sal^{NEt2})N]$^{2+}$** and 1.5% **Mn^{V}(Sal^{NEt2})N** would be present. In addition, the change in $E_{1/2}$ values for the full series of **Mn(Sal^{R})N** complexes correlates with the Hammett parameter of the *para*-ring substituents (Table 1). We note that the Hammett parameter for the R = NEt_2 substituent was estimated to be $\sigma_p = -0.93$ on the basis of previous reports directly comparing this substituent to R = NMe_2 (ref. 88 and 89) and the consensus value for the latter of $\sigma_p = -0.83$.[90] The more negative σ_p for R = NEt_2 in comparison to R = NMe_2 is in agreement with our electrochemistry data.

Spectroscopic characterization

The absorption spectra of the neutral **Mn(Sal^{R})N** complexes are typical of a low spin d^2 square pyramidal complex.[62,63] Upon one-electron oxidation using an equivalent of the $[N(C_5H_3Br_2)_3][SbF_6]$ oxidant (Magic Green) at 193 K, a broad low intensity near infrared (NIR) band is observed at 11 000 cm^{-1} (ε = ~1200 M^{-1} cm^{-1}) for **[Mn(Sal^{H})N]$^+$**, similar to the observed ligand to metal charge transfer (LMCT) transition for **[Mn(Sal^{tBu})N]$^+$** and **[Mn(Sal^{CF3})N]$^+$**, indicating metal-based oxidation (Fig. 2A and S5†).[62] **[Mn(Sal^{H})N]$^+$** was analyzed by electron paramagnetic resonance (EPR) spectroscopy at 20 K, and the EPR spectrum shows a characteristic axial splitting pattern for a d^1 metal ion (d^1_{xy}) with hyperfine coupling to the ^{55}Mn (I = 5/2) nucleus (g_{zz} = 1.986, $g_{xx} = g_{yy}$ = 1.997; A_{zz} = 528 MHz, $A_{xx} = A_{yy}$ = 179 MHz), confirming that one-electron oxidation of **Mn(Sal^{H})N** is metal-based (Fig. 2C). In contrast, for **Mn(Sal^{NEt2})N**, low temperature oxidation affords a unique visible-NIR feature when compared to **[Mn(Sal^{H})N]$^+$**, closely resembling that of **[Mn(Sal^{NMe2})N]$^+$**, indicating ligand-based oxidation (Fig. 2B). The intense envelope of transitions between 15 000 cm^{-1} and 22 000 cm^{-1} are in agreement with ligand radical formation.[62,77,91] The EPR spectrum of a frozen solution of **[Mn(Sal^{NEt2})N]$^+$** exhibits an isotropic signal centered at 2.003, in agreement with ligand-based oxidation (Fig. 2D). Theoretical calculations on the oxidized complexes match the experimental results, predicting a Mn^{VI} (d^1_{xy}) ground state for **[Mn(Sal^{H})N]$^+$** (Fig. S6B†) and a localized ligand radical for **[Mn^{V}(Sal^{NEt2})N]$^{\bullet+}$** as evident by the spin density plots (Fig. 2A and B insets).

Electrophilic reactivity

We next investigated the change in electrophilic reactivity of the full **[Mn(Sal^{R})N]$^+$** series (R =CF_3, H, *t*Bu, O^{i}Pr, NMe_2, NEt_2) *via*

reaction with triarylphosphines. Triphenylphosphine (PPh_3) was initially chosen to probe potential changes in electrophilic reactivity at the nitride. As expected, the neutral **Mn(Sal^{R})N** complexes did not react with PPh_3, as shown by UV-vis-NIR, ESI-MS, and $^{31}P\{H\}$ NMR (Fig. S7–S9†). However, the oxidized **[Mn^{VI}(Sal^{R})N]$^{+}$** complexes (R═CF_3, *t*Bu) react immediately with PPh_3 to form a new species as shown in the low temperature UV-vis-NIR spectroscopy. In contrast, when one equiv. of PPh_3 was added to the ligand radical species (R = NMe_2) at 193 K, a very slow reaction is observed (Fig. S10 and S11†). Unfortunately, the reaction was too fast (completion <1 s) for the Mn^{VI} derivatives to obtain reliable reaction rates under our conditions (Fig. S12†). We therefore investigated the less nucleophilic tris-(trifluoromethylphenyl)phosphine (p-$CF_3Ph)_3P$ to ascertain reactivity differences in this system (Fig. S13†). In addition, we included the full series of Mn salen nitrides with *para*-ring substituents of varying electron-donating ability to provide a more robust Hammett analysis. As expected, the neutral complexes do not react with (p-$CF_3Ph)_3P$ with no change observed in the UV-vis-NIR spectra (Fig. S14†) and ^{31}P NMR (Fig. S15†). However, similarly to the reactivity with PPh_3, the oxidized **[Mn^{VI}(Sal^{R})N]$^{+}$** complexes (R═CF_3, H, *t*Bu, O^{i}Pr) react quickly with (p-$CF_3Ph)_3P$ to form a new species as monitored by UV-vis-NIR measurements at 193 K. Spectral changes, including isosbestic points, indicate clean conversion to a new species for all Mn^{VI} derivatives upon (p-$CF_3Ph)_3P$ addition (Fig. 3A, B and S16†).

The new species (R = *t*Bu) shows minimal decomposition at 193 K over two hours, but decays to a new species upon warming to 298 K (Fig. S17B and S18†). Analysis of the solution at 298 K indicated complete N-atom transfer to form the free iminophosphorane, characterized by the presence of free iminophosphorane [(p-$CF_3Ph)_3PNH$] at ~37 ppm by $^{31}P\{H\}$ NMR with no peak corresponding to unreacted phosphine (Fig. S15 and S19A†). The characterization data is in accord with an independently made sample of the iminophosphorane (Fig. S20†). When 50% ^{15}N labelled nitride complex (R = *t*Bu) was used, a small N–P coupling ($^{1}J_{N-P} = 2.8$ Hz) was observed, with similar $^{1}J_{N-P}$ constants reported for related compounds (Fig. S20A†).[77,92,93] A peak at $m/z = 482$ in positive mode ESI-MS was observed for all derivatives, corresponding to the protonated iminophosphorane [(p-$CF_3Ph)_3PNH_2]^{+}$ (Fig. S19B†). Using 50% ^{15}N labelled nitride complex results in a change in the isotopic pattern consistent with incorporation of the nitride nitrogen (Fig. S19C and D†). In contrast, the reaction of the ligand radical derivatives (R = NMe_2 and NEt_2) with one equivalent of (p-$CF_3Ph)_3P$ is much slower in comparison to the Mn^{VI} analogues (Fig. 3C and S16B†). However, clean conversion to a new species is evident by the presence of the same isosbestic point over a two-hour period. $^{31}P\{H\}$ NMR and ESI-MS analysis after warming to 298 K affords the same iminophosphorane product ($\delta = 37.1$ ppm, $m/z = 482$) (Fig. S21†) as the Mn^{VI} analogues, indicating complete N-atom transfer even for the ligand radical derivatives. Similar results were also observed for the reaction with PPh_3 (Fig. S22 and S23†). We hypothesize that upon warming the solution to 298 K the rate of adduct formation is increased, and in addition, complete N-atom transfer occurs. While complete N-atom transfer was observed for both PPh_3 and (p-$CF_3Ph)_3P$, unlike PPh_3, the reaction rates with (p-$CF_3Ph)_3P$ were amenable to kinetic analysis.

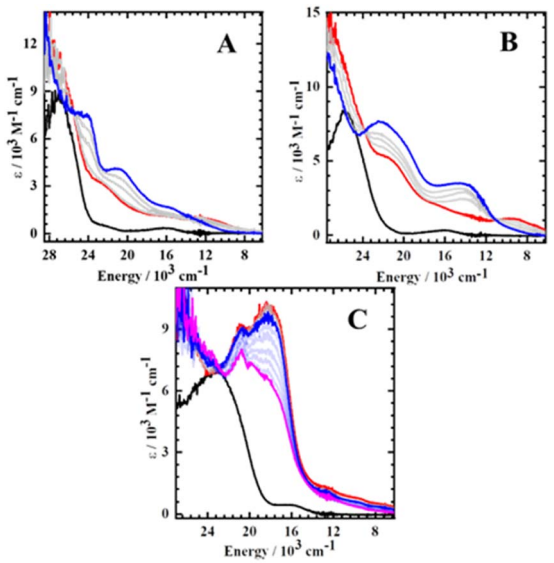

Fig. 3 UV-vis-NIR spectroscopic monitoring of the reaction of (A) [Mn(Sal^{CF3})N]$^{+}$; (B) [Mn(Sal^{tBu})N]$^{+}$; (C) [Mn(Sal^{NMe2})N]$^{+}$ with (p-$CF_3Ph)_3P$. Black: neutral; red: oxidized; blue: one equivalent of (p-$CF_3Ph)_3P$ added to oxidized complexes. Intermediate grey lines measured during aliquot addition of (p-$CF_3Ph)_3P$. For (C) the pink spectrum is 2 h after (p-$CF_3Ph)_3P$ addition, intermediate opaque blue lines are scans taken within two hours. Conditions: CH_2Cl_2, 0.1 mM complex, 193 K. See Fig. S16† for other derivatives.

Kinetic analysis

The Hammett parameter (σ_p) quantifies the electron-donating ability of a *para*-ring substituent and is commonly compared to a rate constant to gain a mechanistic understanding of a particular reaction.[13,87,94] Herein, if the electron-donating capacity of the *para*-ring substituents in **[Mn(Sal^{R})N]$^{+}$** is the main contributor to the nitride reactivity with (p-$CF_3Ph)_3P$, a linear correlation will be expected for all derivatives (R═CF_3, H, *t*Bu, O^{i}Pr, NMe_2, NEt_2), assuming the reaction mechanism remains unchanged.[95,96] However, a substantial deviation from linearity could indicate that the locus of oxidation (metal or ligand), and not the electron-donating ability of a *para*-ring substituent, plays a more significant role in the reaction, in the absence of a change in reaction mechanism. Kinetic measurements under *pseudo*-first order conditions of p-$(CF_3Ph)_3P$ were conducted at 193 K and a substantial difference in reaction rate is observed across all *para*-ring substituents (Fig. S24–S29†), with the R═CF_3 substituted complex reacting fastest, and R = NEt_2 slowest, in line with the relative electron-donating ability of the *para*-ring substituents, and thus suggesting that the nitride is acting as an electrophile (Fig. S30†). Interestingly, a clear reaction rate difference was observed for the high-valent Mn^{VI} complexes (R═CF_3, H, *t*Bu, O^{i}Pr) in comparison to the ligand radical derivatives (R = NMe_2, NEt_2), with the Mn^{VI}

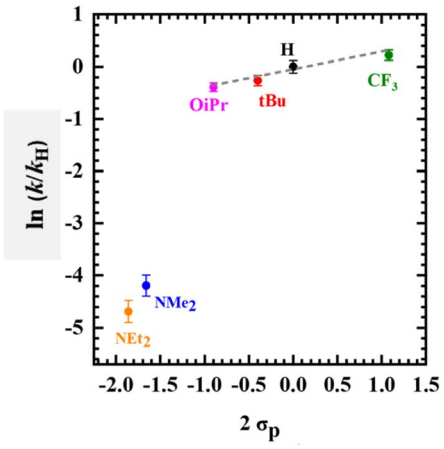

Fig. 4 Hammett plot using k_{obs} for the reaction between oxidized $[Mn(Sal^{R})N]^{+}$ and $(p\text{-}CF_3Ph)_3P$ (R = CF_3, H, *t*Bu, O^iPr, NMe_2, NEt_2). The *x*-axis uses 2 σ_p due to the presence of two R groups in the complex. Note: linear correlation was observed among high-valent Mn^{VI} complexes ($R^2 = 0.95$, $\rho = 0.31$).

complexes reacting much faster (Fig. S30†). A Hammett plot was obtained by graphing $\ln(k/k_H)$ *versus* σ_p (Fig. 4) where k is the observed pseudo first-order rate constant for each Mn-derivative and k_H is the observed pseudo first-order rate constant for $[Mn(Sal^{H})N]^{+}$.[87] A clear break in the plot is observed between the high-valent $[Mn^{VI}(Sal^{R})N]^{+}$ (R=CF_3, H, *t*Bu, O^iPr) complexes and ligand radical $[Mn^{V}(Sal^{R})N]^{\bullet+}$ (R = NMe_2, NEt_2) derivatives. For the Mn^{VI} derivatives, the reaction rates show a linear correlation ($R^2 = 0.95$) with the Hammett parameter ($2\sigma_p$)[87] with a modest reaction constant of $r = 0.31$, indicating that the $[Mn^{VI}(Sal^{R})N]^{+}$ complexes exhibit electrophilic reactivity, and in addition, that the electron-donating ability of the *para*-R substituent plays a relatively minor role in influencing the rate of the reaction.[87] A linear relationship between phosphine concentration and reaction rate was observed for $[Mn^{VI}(Sal^{tBu})N]^{+}$ (Fig. S31 and 32†), indicating that phosphine is involved in the rate law.

Although only two ligand radical derivatives are included in the Hammett plot, the general trend in reactivity suggests that the nitride still exhibits electrophilic reactivity, however the rate is significantly reduced (Fig. S30†). Indeed, further analysis of the reaction rate for $[Mn(Sal^{NMe2})N]^{+\bullet}$ and $(p\text{-}RPh)_3P$, where the donating ability of the phosphine was varied (R = OMe, H, F, and CF_3), shows a negative slope consistent with nucleophilic attack of phosphine at the electrophilic nitride (Fig. S33†). The possibility that the reaction of the oxidized $Mn^{VI}/Mn^{V}L^{\bullet+}$ derivatives could occur *via* outer-sphere single electron transfer (SET) oxidation of PR_3 followed by radical recombination was considered. However, the redox potential required for the first oxidation of both the phosphines are significantly higher in comparison to the Mn complexes indicating that initial SET is unlikely (Fig. S34†). Overall, the Hammett plot shows that the locus of oxidation (metal or ligand) is the dominant factor that determines the rate of reaction between the nitride and phosphine, with the electron-donating ability of the salen *para*-R substituent playing a secondary role.

Adduct characterization

Motivated by stability of the adduct formed between $[Mn(Sal^{tBu})N]^{+}$ and $(p\text{-}CF_3Ph)_3P$ at low temperature in solution (*vide supra*), we endeavored to characterize this species by low temperature EPR spectroscopy. A sample of the reaction mixture at 193 K was transferred to a pre-cooled EPR tube and immediately frozen for further analysis. EPR spectra (R = CF_3, *t*Bu, O^iPr, H, NMe_2) of the reaction mixture for each of the oxidized complexes and $(p\text{-}CF_3Ph)_3P$ shows features in the low field region at $g \sim 5.2$ and 3.7 consistent with the expected Mn^{IV} phosphoraneiminato adduct (Fig. 5).[97,98] For the R = NMe_2 derivative, the relatively weak Mn^{IV} features in comparison to the strong signal at $g = 2.003$ is consistent with the slow reactivity for the ligand radical complex as measured by UV-vis-NIR spectroscopy (Fig. 3C). For R = *t*Bu, additional features indicating unreacted oxidized Mn nitride complex ($g \sim 2.0$) and a minor Mn^{III} species at $g \sim 7.3$,[97,99] highlight the instability of the adduct, and possible background nitride homocoupling reaction.[62]

We suspect these additional species are a result of the EPR sample preparation, and due to the presence of multiple Mn species we did not attempt to simulate the spectra. However, when the Mn^{VI} and Mn^{III} EPR spectra were subtracted from the adduct spectrum for the *t*Bu derivative, the resultant spectrum (Fig. S35†) closely resembles EPR data reported by Fujii *et al.* for Mn^{IV}(Sal)–Cl and Mn^{IV}(Sal)–OH.[97,98] This is in agreement with the UV-vis-NIR data (Fig. 3A and B), with new features for the Mn^{IV} phosphoraneiminato adducts consistent with previously reported Mn^{IV} complexes.[97,98] To further evaluate the decay

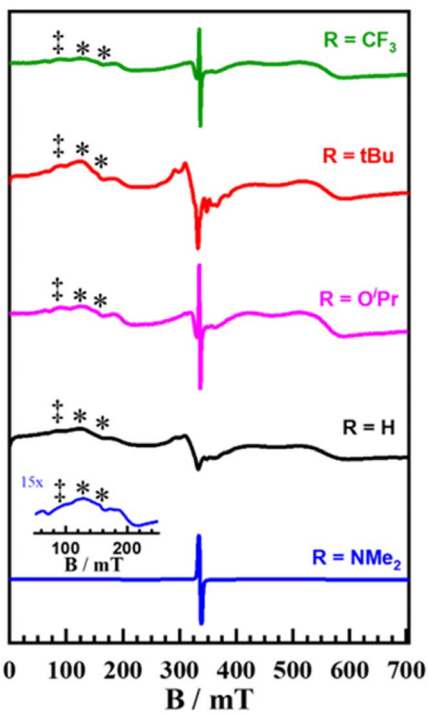

Fig. 5 X-band EPR spectra of frozen samples of $[Mn(Sal^{R})N]^{+}$ + $(p\text{-}CF_3Ph)_3P$. (‡ Mn^{III} feature: $g = 7.3$; * Mn^{IV} features: $g = 5.2$ and 3.7) Conditions: frequency = 9.38 GHz; power = 2.0 mW; modulation frequency = 100 kHz; modulation amplitude = 0.6 mT; $T = 4$ K.

process of the adduct we analyzed the EPR spectrum of the reaction mixture for **[Mn(Sal^{tBu})N]$^+$** and $(p\text{-}CF_3Ph)_3P$ after warming to 298 K. We observe an increase in the Mn^{III} signal at g ~7.3, and a decrease in the signals associated with the Mn^{IV} adduct at ~5.2 and 3.7 (Fig. S36†). EPR analysis of independently prepared **[Mn^{III}(Sal^{tBu})Cl]** at 4 K shows a significant feature at g ~7.3, further corroborating the assignment of a similar species in the adduct and decay spectra. The eventual formation of the Mn^{III} complex is consistent with N-atom transfer from the metal complex to $(p\text{-}CF_3Ph)_3P$, in accord with the NMR and MS analysis (*vide supra*), and subsequent reduction of the resulting Mn^{IV} complex by either impurities or excess phosphine.[77]

Theoretical calculations

Theoretical calculations were used to further understand the electronic structure of the oxidized Mn complexes and observed reactivity differences with phosphine. In accord with experimental data, calculations on the one-electron oxidized complexes predict a Mn^{VI} electronic ground state for R = CF_3, *t*Bu, O^{i}Pr, H, while a Mn^V ligand radical ground state was predicted for R = NMe_2, NEt_2 (*vide supra*).[62,63] We next evaluated the difference in nitride NPA charge between the neutral and oxidized forms, with the Mn^{VI} derivatives exhibiting a much more significant increase in nitride NPA charge and therefore electrophilicity upon oxidation in comparison to the Mn^V ligand radical derivatives (Fig. 6). In addition, we observe an expected decrease in energy of the Mn≡N π* orbitals upon oxidation. However, the relative decrease in energy for the Mn^{VI} derivatives is larger (*ca.* −68 kcal mol^{-1}) in comparison to the Mn^V ligand radical analogues (*ca.* −38 kcal mol^{-1}), implying that the empty Mn≡N π* orbitals for the Mn^{VI} derivatives are energetically more accessible to reaction with a nucleophile (Fig. 6).

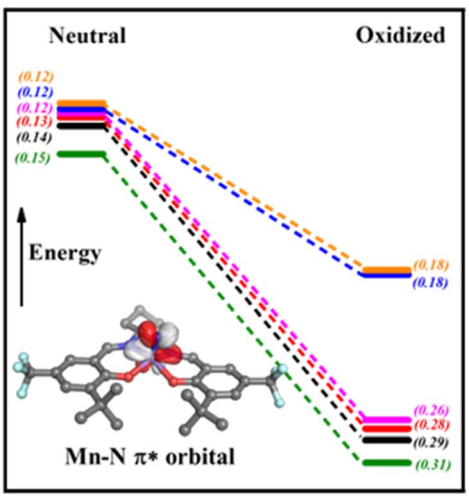

Fig. 6 Change in predicted Mn≡N π* orbital energies upon oxidation for **Mn(Sal^R)N** complexes from natural bond order (NBO) analysis. Green (R = CF_3), black (R = H), red (R = *t*Bu), purple (R = O^{i}Pr), blue (R = NMe_2), orange (R = NEt_2). The Mn≡N π* orbital energies are lower by −68.5 kcal mol^{-1} (CF_3, Mn^{VI}), by −68.7 kcal mol^{-1} (H, Mn^{VI}), −69.0 kcal mol^{-1} (*t*Bu, Mn^{VI}), −68.0 kcal mol^{-1} (O^{i}Pr, Mn^{VI}), −36.8 kcal mol^{-1} (NMe_2, $Mn^VL^{\bullet+}$), −37.0 kcal mol^{-1} (NEt_2, $Mn^VL^{\bullet+}$) in comparison to the neutral analogues. NPA charge on nitride N in brackets, indicating degree of electrophilic character.

We next investigated the reaction profile of the neutral and oxidized Mn complexes with $(p\text{-}CF_3Ph)_3P$. As expected, the neutral complexes exhibit high transition state energies for adduct formation and the resulting bent triplet phosphoraneiminato products are de-stabilized by *ca.* 16–21 kcal mol^{-1} in comparison to the reactants (Table S2, Fig. S37 and S38†). This data is in agreement with the lack of reaction observed experimentally. In contrast, calculations predict that bent Mn^{IV} phosphoraneiminato adducts formed for all six **[Mn(Sal^R)N]$^+$** complexes with $(p\text{-}CF_3Ph)_3P$ are stabilized in comparison to the isolated reactants, with the trend in stability following the electron-donating ability of the *para*-ring substituents (Fig. 7 and Table S3†). Calculations predict the high spin quartet state to be of lowest energy (Table S3†), with unpaired electrons in d_{xy}, d_{xz}, and d_{yz} orbitals (Fig. S39 and S40†). This is in agreement with the EPR data for the adducts. Analysis of both the doublet and quartet reaction profiles supports that the transition state (TS) is located on the doublet surface with spin-crossover to the quartet state occurring after the TS (Fig. S41†). Indeed, a minimum energy crossing potential (MECP)[100–102] calculation for the **[Mn(Sal^{CF3})N]$^+$** derivative predicts the spin-crossover to occur at 2.16 Å, with the TS at 2.34 Å, in agreement with the relaxed potential energy surface scan. The calculated TS energies for the **[Mn(Sal^R)N]$^+$** complexes are significantly lower in energy in comparison to the neutral complexes (Fig. 7). However, the high-valent Mn^{VI} derivatives exhibit TS of lower energy (11.9–14.4) kcal mol^{-1} when compared to the Mn^V ligand radical analogues (20.7–21.2 kcal mol^{-1}) (Fig. 7 and Table S2†). Analysis of the adduct geometry at the TS for all the oxidized derivatives predicts a bent approach of the phosphine nucleophile with a Mn–N–P bond angle of *ca.* 135° (Fig. S42†). Two different orbital interactions are possible, including phosphorous (P) lone pair (lp) donation into a vacant Mn≡N π* orbital, or alternatively donation by a filled nitride N lp orbital into a P–C σ* orbital (Fig. S43†).[87] Further analysis of adduct formation at constrained P–N distances for both **[Mn(Sal^{tBu})N]$^+$** and **[Mn(Sal^{NMe2})N]$^{\bullet+}$** predicts a decrease in P lp occupancy and a concomitant increase in Mn≡N π* occupancy as the reactants approach the TS (Tables S5 and S6†). In contrast, the nitride N lp and P–C σ* orbital occupancies remain unchanged, thereby supporting nucleophilic attack of the phosphine on an electrophilic nitride (Tables S5 and S6†). Additional examination of the adduct formation at fixed P–N distances predicts a rise in the NPA charge on the phosphine coupled with a corresponding reduction in the NPA charge on **[Mn(Sal^R)N]$^+$** (R = CF_3 and NMe_2) as the distance between the reactants is decreased. This observation is consistent with the empirical findings, which demonstrate a nucleophilic interaction of the phosphine with an electrophilic nitride (Tables S5 and S6†).[55] Moreover, a similar trend for both the Mn^{VI} and the Mn^V ligand radical derivatives indicates a similar reaction mechanism. For the high-valent Mn^{VI} complexes, the lowest energy transition state is predicted for the least donating *para*-ring substituent (R = CF_3), with a trend in increasing TS energy with increasing

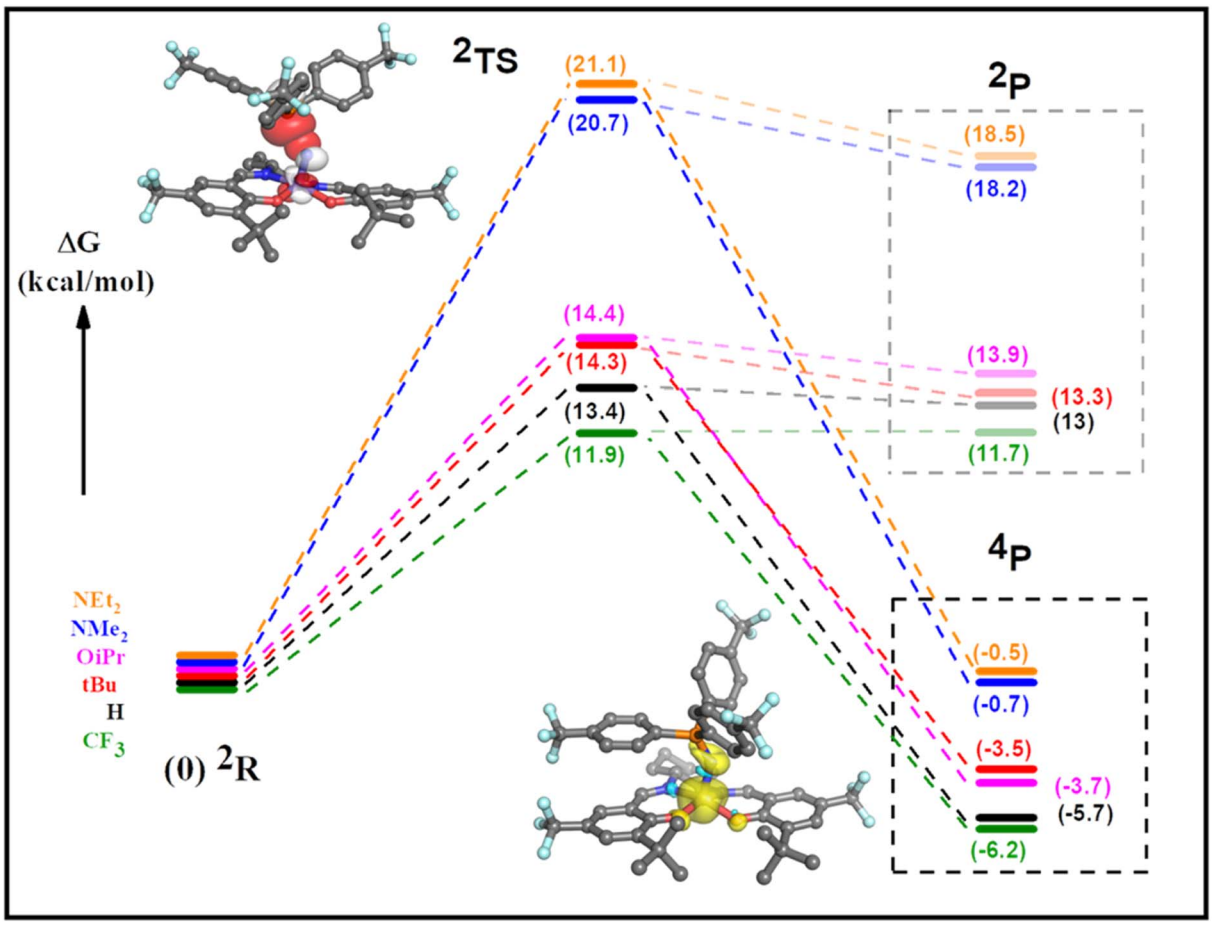

Fig. 7 Predicted reaction profiles for $[Mn(Sal^{R})N]^{+}$ and $(p\text{-}CF_3Ph)_3P$ to form a bent Mn^{IV} phosphoraneiminato adduct. The initial doublet spin state (^{2}R) proceeds through the transition state (^{2}TS) before crossing to the quartet surface and forming the bent Mn^{IV} adduct (^{4}P). Note the predicted product on the doublet surface (^{2}P) is considerably higher in energy. Insets: top left, DFT-computed TS for $[Mn(Sal^{CF3})N]^{+}$ and $(p\text{-}CF_3Ph)_3P$, including overlap of Mn≡N π* and P lone pair orbitals; bottom right, bent quartet adduct for $[Mn(Sal^{CF3})N]^{+}$ and $(p\text{-}CF_3Ph)_3P$, including spin density. Refer to the experimental section for calculation details.

electron-donating ability of the *para*-ring substituent (Fig. 7). The trend in predicted TS energies matches the experimentally observed trend in reaction rates. In addition, the relatively small difference in predicted TS energies for the Mn^{VI} complexes, and the significantly larger TS energies for the Mn^{V} ligand radical analogues, suggests that the locus of oxidation is the major determinant of the observed reactivity. Theoretical k/k_H values were obtained by imputing DFT-calculated activation energies into the Eyring equation (see ESI† for details), and the resulting predicted Hammett plot presents a clear difference in reactivity between the high-valent $[Mn^{VI}(Sal^{R})N]^{+}$ (R = CF_3, H, *t*Bu, O^iPr) complexes and ligand radical $[Mn^{V}(Sal^{R})N]^{\cdot+}$ (R = NMe_2, NEt_2) derivatives. Additionally, among the Mn^{VI} derivatives, the reaction rates show a linear correlation (R^2 = 0.93) with the Hammett parameter ($2\sigma_p$) as observed experimentally (Fig. S44†).

Summary

In this study we investigated how electronic structure influences electrophilic nitride reactivity in a series of oxidized Mn salen nitrides. More specifically, we explored if the locus of oxidation (metal or ligand) was the major factor dictating reactivity at the nitride, or whether this was secondary to the overall electron-donating ability of the ancillary salen ligands. Changing the *para*-ring substituent of the ancillary salen ligand provided a means to change the electronic structure without significantly altering the geometry at the metal center. In addition to previously synthesized complexes, two new $Mn(Sal^{R})N$ (R = H and NEt_2) complexes were synthesized and thoroughly characterized. One-electron oxidation of $Mn(Sal^{H})N$ affords a high-valent Mn^{VI} species whereas oxidation of $Mn(Sal^{NEt2})N$ affords a ligand radical, as shown by spectroscopic experiments and supported by DFT calculations. Reactivity of the extended series of neutral $Mn(Sal^{R})N$ and mono-oxidized $[Mn(Sal^{R})N]^{+}$ (R = CF_3, H, *t*Bu, O^iPr, NMe_2, NEt_2) complexes with PPh_3 and $(p\text{-}CF_3Ph)_3P$ was then investigated to probe for differences in electrophilic nitride reactivity. While the neutral complexes are unreactive towards PPh_3 and $(p\text{-}CF_3Ph)_3P$, the oxidized complexes react at the nitride to form a bent Mn^{IV} phosphoraneiminato adduct. The adduct was identified by low temperature EPR measurements, however, upon warming to 298 K complete N-atom

transfer occurs to form the free iminophosphorane and a Mn^{III} complex. Kinetic analysis of the reaction of the full series of $[Mn(Sal^R)N]^+$ complexes with triarylphosphines proves that the locus of oxidation is the most significant factor in determining the electrophilic reactivity at the nitride, as established by a break in the Hammett plot between high-valent Mn^{VI} and Mn^{V} ligand radical complexes. Experimental observations are further supported by theoretical calculations in terms of the electronic structure reactivity profile. This work has motivated us to investigate the possibility of C–H bond activation by the more electrophilic nitrides of the $[Mn(Sal^R)N]^+$ series.

Data availability

The computational details supporting this article have been uploaded as part of the ESI.†

Author contributions

S. M. synthesized and characterized all compounds, performed all CV experiments, collected UV-vis-NIR spectra, acquired kinetic data, and performed computational analysis with T. S. EPR data was collected by G. A. M. and W. V. simulated the data. Crystallographic data was refined by J. M. P. The manuscript was written by S. M. and T. S.

Conflicts of interest

There are no conflicts to declare.

Acknowledgements

This work was supported by Natural Sciences and Engineering Research Council (NSERC) Discovery Grants (RGPIN-2019-06749 and RGPAS-2019-00054 to T. S.). The Digital Research Alliance of Canada is thanked for access to computational resources. S. M thanks Mitacs for Globalink Graduate Fellowship (GLF599). W. V. and G. A. M. acknowledge NSERC for postgraduate fellowships. The authors thank Prof. Charles Walsby for access to the EPR instrument. Professor Fabrice Thomas (Grenoble) is thanked for insightful discussions on this work.

Notes and references

1 D. V. Yandulov and R. R. Schrock, *Science*, 2003, **301**(5629), 76–78.
2 K. Arashiba, E. Kinoshita, S. Kuriyama, A. Eizawa, K. Nakajima, H. Tanaka, K. Yoshizawa and Y. Nishibayashi, *J. Am. Chem. Soc.*, 2015, **137**(17), 5666–5669.
3 J. S. Anderson, J. Rittle and J. C. Peters, *Nature*, 2013, **501**(7465), 84–87.
4 S. J. K. Forrest, B. Schluschaß, E. Y. Yuzik-Klimova and S. Schneider, *Chem. Rev.*, 2021, **121**(11), 6522–6587.
5 M. N. Cosio and D. C. Powers, *Nat. Rev. Chem.*, 2023, **7**(6), 424–438.
6 J. J. Curley, E. L. Sceats and C. C. Cummins, *J. Am. Chem. Soc.*, 2006, **128**(43), 14036–14037.
7 J. Du Bois, C. S. Tomooka, J. Hong and E. M. Carreira, *Acc. Chem. Res.*, 1997, **30**(9), 364–372.
8 R. L. Gdula and M. J. Johnson, *J. Am. Chem. Soc.*, 2006, **128**(30), 9614–9615.
9 M. H. Chisholm, E. E. Delbridge, A. R. Kidwell and K. B. Quinlan, *Chem. Commun.*, 2003, **1**, 126–127.
10 S. Wang, H. Ge, S. Sun, J. Zhang, F. Liu, X. Wen, X. Yu, L. Wang, Y. Zhang, H. Xu, J. C. Neuefeind, Z. Qin, C. Chen, C. Jin, Y. Li, D. He and Y. Zhao, *J. Am. Chem. Soc.*, 2015, **137**(14), 4815–4822.
11 T.-N. Ye, S.-W. Park, Y. Lu, J. Li, M. Sasase, M. Kitano and H. Hosono, *J. Am. Chem. Soc.*, 2020, **142**(33), 14374–14383.
12 R. A. Karaballi, G. Humagain, B. R. A. Fleischman and M. Dasog, *Angew. Chem., Int. Ed.*, 2019, **58**(10), 3147–3150.
13 J. J. Scepaniak, C. S. Vogel, M. M. Khusniyarov, F. W. Heinemann, K. Meyer and J. M. Smith, *Science*, 2011, **331**(6020), 1049–1052.
14 C. Vogel, F. W. Heinemann, J. Sutter, C. Anthon and K. Meyer, *Angew. Chem., Int. Ed.*, 2008, **47**(14), 2681–2684.
15 J. U. Rohde, T. A. Betley, T. A. Jackson, C. T. Saouma, J. C. Peters and L. Que, *Inorg. Chem.*, 2007, **46**(14), 5720–5726.
16 N. Aliaga-Alcalde, S. DeBeer George, B. Mienert, E. Bill, K. Wieghardt and F. Neese, *Angew. Chem.*, 2005, **117**(19), 2968–2972.
17 K. Meyer, J. Bendix, N. Metzler-Nolte, T. Weyhermüller and K. Wieghardt, *J. Am. Chem. Soc.*, 1998, **120**(29), 7260–7270.
18 J. F. Berry, E. Bill, E. Bothe, S. D. George, B. Mienert, F. Neese and K. Wieghardt, *Science*, 2006, **312**(5782), 1937–1941.
19 J. J. Scepaniak, R. P. Bontchev, D. L. Johnson and J. M. Smith, *Angew. Chem., Int. Ed.*, 2011, **50**(29), 6630–6633.
20 S. B. Munoz, W. T. Lee, D. A. Dickie, J. J. Scepaniak, D. Subedi, M. Pink, M. D. Johnson and J. M. Smith, *Angew. Chem., Int. Ed.*, 2015, **54**(36), 10600–10603.
21 S. Aghazada, M. Miehlich, J. Messelberger, F. W. Heinemann, D. Munz and K. Meyer, *Angew. Chem., Int. Ed.*, 2019, **58**(51), 18547–18551.
22 N. B. Thompson, M. T. Green and J. C. Peters, Nitrogen Fixation via a Terminal Fe(IV) Nitride, *J. Am. Chem. Soc.*, 2017, **139**(43), 15312–15315.
23 A. K. Maity, J. Murillo, A. J. Metta-Magaña, B. Pinter and S. Fortier, *J. Am. Chem. Soc.*, 2017, **139**, 15691–15700.
24 T. J. Del Castillo, N. B. Thompson and J. C. Peters, *J. Am. Chem. Soc.*, 2016, **138**(16), 5341–5350.
25 J. J. Scepaniak, M. D. Fulton, R. P. Bontchev, E. N. Duesler, M. L. Kirk and J. M. Smith, *J. Am. Chem. Soc.*, 2008, **130**(32), 10515–10517.
26 T. A. Betley and J. C. Peters, *J. Am. Chem. Soc.*, 2004, **126**, 6252–6254.
27 M. Keilwerth, L. Grunwald, W. Mao, F. W. Heinemann, J. Sutter, E. Bill and K. Meyer, *J. Am. Chem. Soc.*, 2021, **143**(3), 1458–1465.
28 A. McSkimming and D. L. M. Suess, *Nat. Chem.*, 2021, **13**(7), 666–670.

29 A. Sridharan, A. C. Brown and D. L. M. Suess, *Angew. Chem., Int. Ed.*, 2021, **60**(23), 12802–12806.
30 J. M. Smith, *Prog. Inorg. Chem.*, 2014, **58**, 417–470.
31 R. A. Eikey and M. M. Abu-Omar, *Coord. Chem. Rev.*, 2003, **243**(1–2), 83–124.
32 J. F. Berry, *Comments Inorg. Chem.*, 2009, **30**(1–2), 28–66.
33 A. G. Maestri, K. S. Cherry, J. J. Toboni and S. N. Brown, *J. Am. Chem. Soc.*, 2001, **123**(30), 7459–7460.
34 T. J. Crevier, S. Lovell, J. M. Mayer, A. L. Rheingold and I. A. Guzei, *J. Am. Chem. Soc.*, 1998, **120**(26), 6607–6608.
35 T. J. Crevier, B. K. Bennett, J. D. Soper, J. A. Bowman, A. Dehestani, D. A. Hrovat, S. Lovell, W. Kaminsky and J. M. Mayer, *J. Am. Chem. Soc.*, 2001, **123**, 1059–1071.
36 T. J. Meyer and M. H. V. Huynh, *Inorg. Chem.*, 2003, **42**(25), 8140–8160.
37 W.-L. Man, W. W. Y. Lam, H.-K. Kwong, S.-M. Yiu and T.-C. Lau, *Angew. Chem., Int. Ed.*, 2012, **51**, 9101–9104.
38 W.-L. Man, T.-M. Tang, T.-W. Wong, T.-C. Lau, S.-M. Peng and W.-T. Wong, *J. Am. Chem. Soc.*, 2004, **126**(2), 478–479.
39 W. L. Man, W. W. Y. Lam, S. M. Yiu, T. C. Lau and S. M. Peng, *J. Am. Chem. Soc.*, 2004, **126**, 15336–15337.
40 E. M. Zolnhofer, M. Käß, M. M. Khusniyarov, F. W. Heinemann, L. Maron, M. van Gastel, E. Bill and K. Meyer, *J. Am. Chem. Soc.*, 2014, **136**, 15072–15078.
41 M. G. Scheibel, Y. L. Wu, A. C. Stuckl, L. Krause, E. Carl, D. Stalke, B. de Bruin and S. Schneider, *J. Am. Chem. Soc.*, 2013, **135**(47), 17719–17722.
42 J. Schoffel, A. Y. Rogachev, S. DeBeer George and P. Burger, *Angew. Chem.*, 2009, **48**(26), 4734–4738.
43 T. Schmidt-Räntsch, H. Verplancke, J. N. Lienert, S. Demeschko, M. Otte, G. P. Van Trieste III, K. A. Reid, J. H. Reibenspies, D. C. Powers, M. C. Holthausen and S. Schneider, *Angew. Chem., Int. Ed.*, 2022, **61**, e2021156.
44 V. Vreeken, M. A. Siegler, B. de Bruin, J. N. Reek, M. Lutz and J. I. van der Vlugt, *Angew. Chem.*, 2015, **54**(24), 7055–7059.
45 M. G. Scheibel, B. Askevold, F. W. Heinemann, E. J. Reijerse, B. de Bruin and S. Schneider, *Nat. Chem.*, 2012, **4**(7), 552–558.
46 C. E. Laplaza and C. C. Cummins, *Science*, 1995, **268**(5212), 861–863.
47 C. E. Laplaza, M. J. A. Johnson, J. C. Peters, A. L. Odom, E. Kim, C. C. Cummins, G. N. George and I. J. Pickering, *J. Am. Chem. Soc.*, 1996, **118**(36), 8623–8638.
48 J. J. Curley, T. R. Cook, S. Y. Reece, P. Muller and C. C. Cummins, *J. Am. Chem. Soc.*, 2008, **130**(29), 9394–9405.
49 R. Thompson, B. L. Tran, S. Ghosh, C. H. Chen, M. Pink, X. Gao, P. J. Carroll, M. H. Baik and D. Mindiola, *J. Inorg. Chem.*, 2015, **54**(6), 3068–3077.
50 L. N. Grant, M. Bhunia, B. Pinter, C. Rebreyend, M. E. Carroll, P. J. Carroll, B. de Bruin and D. Mindiola, *J. Inorg. Chem.*, 2021, **60**(8), 5635–5646.
51 L. N. Grant, B. Pinter, T. Kurogi, M. E. Carroll, G. Wu, B. C. Manor, P. J. Carroll and D. J. Mindiola, *Chem. Sci.*, 2017, **8**(2), 1209–1224.
52 L. N. Grant, B. Pinter, J. Gu and D. J. Mindiola, *J. Am. Chem. Soc.*, 2018, **140**(50), 17399–17403.
53 T. Kurogi, P. J. Carroll and D. J. Mindiola, *J. Am. Chem. Soc.*, 2016, **138**(13), 4306–4309.
54 H. Shi, H. K. Lee, Y. Pan, K.-C. Lau, S.-M. Yiu, W. W. Y. Lam, W.-L. Man and T.-C. Lau, *J. Am. Chem. Soc.*, 2021, **143**(38), 15863–15872.
55 F. S. Schendzielorz, M. Finger, C. Volkmann, C. Würtele and S. Schneider, *Angew. Chem., Int. Ed.*, 2016, **55**(38), 11417–11420.
56 D. Sieh and P. Burger, *J. Am. Chem. Soc.*, 2013, **135**(10), 3971–3982.
57 T. J. Crevier and J. M. Mayer, *J. Am. Chem. Soc.*, 1998, **120**, 5595–5596.
58 A. Dehestani, W. Kaminsky and J. M. Mayer, *Inorg. Chem.*, 2003, **42**(2), 605–611.
59 T.-W. Wong, T.-C. Lau and W.-T. O. Wong, *Inorg. Chem.*, 1999, **38**(26), 6181–6186.
60 G. P. Connor, B. Q. Mercado, H. M. C. Lant, J. M. Mayer and P. L. Holland, *Inorg. Chem.*, 2019, **58**(16), 10791–10801.
61 C. Schiller, D. Sieh, N. Lindenmaier, M. Stephan, N. Junker, E. Reijerse, A. A. Granovsky and P. Burger, *J. Am. Chem. Soc.*, 2023, **145**(20), 11392–11401.
62 R. M. Clarke and T. Storr, *J. Am. Chem. Soc.*, 2016, **138**(47), 15299–15302.
63 N. M. Hein, G. A. MacNeil and T. Storr, *Inorg. Chem.*, 2021, **60**(22), 16895–16905.
64 Y. Shimazaki, F. Tani, K. Fukui, Y. Naruta and O. Yamauchi, *J. Am. Chem. Soc.*, 2003, **125**, 10512–10513.
65 T. Kurahashi and H. Fujii, *J. Am. Chem. Soc.*, 2011, **133**(21), 8307–8316, DOI: **10.1021/ja2016813**.
66 L. Chiang, K. Herasymchuk, F. Thomas and T. Storr, *Inorg. Chem.*, 2015, **54**(12), 5970–5980.
67 R. M. Clarke, K. Herasymchuk and T. Storr, *Coord. Chem. Rev.*, 2017, **352**, 67–82.
68 J. Andrez, V. Guidal, R. Scopelliti, J. Pécaut, S. Gambarelli and M. Mazzanti, *J. Am. Chem. Soc.*, 2017, **139**, 8628–8638.
69 T. Storr, E. C. Wasinger, R. C. Pratt and T. D. P. Stack, *Angew. Chem., Int. Ed.*, 2007, **46**, 5198–5201.
70 M. Orio, O. Jarjayes, H. Kanso, C. Philouze, F. Neese and F. Thomas, *Angew. Chem., Int. Ed.*, 2010, **49**, 4989–4992.
71 M. Keener, M. Peterson, R. Hernández Sánchez, V. F. Oswald, G. Wu and G. Ménard, *Chem.–Eur. J.*, 2017, **23**(48), 11479–11484.
72 T. Chantarojsiri, A. H. Reath and J. Y. Yang, *Angew. Chem., Int. Ed.*, 2018, **57**(43), 14037–14042.
73 N. G. Léonard, T. Chantarojsiri, J. W. Ziller and J. Y. Yang, *J. Am. Chem. Soc.*, 2022, **144**(4), 1503–1508.
74 S. Kim, H. Y. Zhong, Y. Park, F. Loose and P. J. Chirik, *J. Am. Chem. Soc.*, 2020, **142**(20), 9518–9524.
75 F. Loose, D. A. Wang, L. Tian, G. D. Scholes, R. R. Knowles and P. J. Chirik, *Chem. Commun.*, 2019, **55**(39), 5595–5598.
76 H. Toda, K. Kuroki, R. Kanega, S. Kuriyama, K. Nakajima, Y. Himeda, K. Sakata and Y. Nishibayashi, *Chempluschem*, 2021, **86**(11), 1511–1516.
77 D. Martelino, S. Mahato, W. VandeVen, N. M. Hein, R. M. Clarke, G. A. MacNeil, F. Thomas and T. Storr, *J. Am. Chem. Soc.*, 2022, **144**(26), 11594–11607.

78 D. D. Dumez and J. M. Mayer, *Inorg. Chem.*, 1995, **34**(25), 6396–6401.
79 D. D. DuMez and J. M. Mayer, *Inorg. Chem.*, 1998, **37**(3), 445–453.
80 S. B. Seymore and S. N. Brown, *Inorg. Chem.*, 2000, **39**, 325–332.
81 S. N. Brown and J. M. Mayer, *J. Am. Chem. Soc.*, 1996, **118**(48), 12119–12133.
82 R. H. Holm, *Chem. Rev.*, 1987, **87**(6), 1401–1449.
83 Y. M. Lee, M. Yoo, H. Yoon, X. X. Li, W. Nam and S. Fukuzumi, *Chem. Commun.*, 2017, **53**(67), 9352–9355.
84 B. K. Bennett, E. Saganic, S. Lovell, W. Kaminsky, A. Samuel and J. M. Mayer, *Inorg. Chem.*, 2003, **42**, 4127–4134.
85 X. Y. Yi, T. C. H. Lam, Y.-K. Sau, Q.-F. Zhang, I. D. Williams and W.-H. Leung, *Inorg. Chem.*, 2007, **46**, 7193–7198.
86 C. Besson, Y. V. Geletii, F. Villain, R. Villanneau, C. L. Hill and A. Proust, *Inorg. Chem.*, 2009, **48**, 9436–9443.
87 J. J. Scepaniak, C. G. Margarit, J. N. Harvey and J. M. Smith, *Inorg. Chem.*, 2011, **50**(19), 9508–9517.
88 C. C. Price and W. J. Belanger, *J. Am. Chem. Soc.*, 1954, **76**(10), 2682–2684.
89 W. G. Herkstroeter, *J. Am. Chem. Soc.*, 1973, **95**(26), 8686–8691.
90 C. Hansch, A. Leo and R. W. Taft, *Chem. Rev.*, 1991, **91**(2), 165–195.
91 K. Herasymchuk, L. Chiang, C. E. Hayes, M. L. Brown, J. S. Ovens, B. O. Patrick, D. B. Leznoff and T. Storr, *Dalton Trans.*, 2016, **45**(31), 12576–12586.
92 G. Zhang, T. Liu, J. Song, Y. Quan, L. Jin, M. Si and Q. Liao, *J. Am. Chem. Soc.*, 2022, **144**, 2444–2449.
93 C. Lopez-Leonardo, M. Alajarin, P. Llamas-Lorente, D. Bautista, M. L. Jimeno, I. Alkorta and J. Elguero, *Struct. Chem.*, 2003, **14**(4), 391–397.
94 B. E. Nadeau, D. D. Beattie, E. K. J. Lui, M. Tewkesbury, J. A. Love and L. L. Schafer, *Organometallics*, 2023, **42**(17), 2326–2334.
95 M. J. Zdilla, J. L. Dexheimer and M. M. Abu-Omar, *J. Am. Chem. Soc.*, 2007, **129**(37), 11505–11511.
96 H. M. Neu, T. Yang, R. A. Baglia, T. H. Yosca, M. T. Green, M. G. Quesne, S. P. de Visser and D. P. Goldberg, *J. Am. Chem. Soc.*, 2014, **136**(39), 13845–13852.
97 T. Kurahashi, A. Kikuchi, T. Tosha, Y. Shiro, T. Kitagawa and H. Fujii, *Inorg. Chem.*, 2008, **47**(5), 1674–1686.
98 T. Kurahashi, A. Kikuchi, Y. Shiro, M. Hada and H. Fujii, *Inorg. Chem.*, 2010, **49**(14), 6664–6672.
99 K. A. Campbell, M. R. Lashley, J. K. Wyatt, M. H. Nantz and R. D. Britt, *J. Am. Chem. Soc.*, 2001, **123**(24), 5710–5719.
100 P. L. Holland, *Acc. Chem. Res.*, 2015, **48**, 1696.
101 T. Yang, M. G. Quesne, H. M. Neu, F. G. CantúReinhard, D. P. Goldberg and S. P. de Visser, *J. Am. Chem. Soc.*, 2016, **138**, 12375.
102 R. Poli and J. N. Harvey, *Chem. Soc. Rev.*, 2003, **32**, 1.